

HOT GALACTIC WINDS CONSTRAINED BY THE X-RAY LUMINOSITIES OF GALAXIES

DONG ZHANG^{1,2}, TODD A. THOMPSON^{1,2}, NORMAN MURRAY^{3,5}, AND ELIOT QUATAERT⁴

Draft version August 23, 2021

ABSTRACT

Galactic superwinds may be driven by very hot outflows generated by overlapping supernovae within the host galaxy. We use the Chevalier & Clegg (CC85) wind model and the observed correlation between X-ray luminosities of galaxies and their SFRs to constrain the mass-loss rates (\dot{M}_{hot}) across a wide range of star formation rates (SFRs), from dwarf starbursts to ultra-luminous infrared galaxies. We show that for fixed thermalization and mass-loading efficiencies, the X-ray luminosity of the hot wind scales as $L_X \propto \text{SFR}^2$, significantly steeper than is observed for star-forming galaxies: $L_X \propto \text{SFR}$. Using this difference we constrain the mass-loading and thermalization efficiency of hot galactic winds. For reasonable values of the thermalization efficiency ($\lesssim 1$) and for $\text{SFR} \gtrsim 10 M_\odot \text{ yr}^{-1}$ we find that $\dot{M}_{\text{hot}}/\text{SFR} \lesssim 1$, significantly lower than required by integrated constraints on the efficiency of stellar feedback in galaxies, and potentially too low to explain observations of winds from rapidly star-forming galaxies. In addition, we highlight the fact that heavily mass-loaded winds cannot be described by the adiabatic CC85 model because they become strongly radiative.

Subject headings: galaxies: evolution — galaxies: star formation — galaxies: fundamental parameters — galaxies: starburst — X-rays: galaxies

1. INTRODUCTION

Galactic-scale winds are important in rapidly star-forming galaxies. They are the primary mechanism by which energy and metals are ejected from galaxies and deposited into the intergalactic medium, and they are a product of the feedback mechanisms at work in regulating star formation.

A number of mechanisms have been proposed for launching galactic superwinds, including energy and momentum deposition by supernovae (SN), radiation pressure on dust, and cosmic rays (Dekel & Silk 1986; Murray et al. 2005; Everett et al. 2008; Socrates et al. 2008; Hopkins et al. 2012). Chevalier & Clegg (1985) (hereafter CC85) developed a one-dimensional (1D) spherically-symmetric model for a very hot wind created by supernova energy injection with two controlling parameters: the thermalization efficiency with which SN energy is converted into thermal energy, and the mass-loading efficiency. Numerical simulations show that this analytic model provides a good approximation in describing the hot wind fluid properties and emission from axisymmetric disk-like configurations (Strickland & Heckman 2009), or in three-dimensional starburst models (Stevens & Hartwell 2003).

The thermalization efficiency and, in particular, the mass-loading efficiency are the crucial parameters that determine the overall importance of hot winds in driving matter and metals out of galaxies. Higher thermalization efficiencies imply higher velocities and higher temperatures, and larger mass-loading rates imply more hot wind momentum available to accelerate cold clouds. Despite their importance these parameters are difficult to determine observationally. Both low

(e.g., Bradamante et al. 1998) and high thermalization efficiency (e.g., Strickland & Stevens 2000) have been inferred. Constraints on the mass-loss rate of the hot flow (\dot{M}_{hot}) in individual galaxies by observation are few, e.g., NGC 1569 (Martin et al. 2002), and M82 (Strickland & Heckman 2009).

One method to constrain the hot wind properties directly is by X-ray observations. Recently, Strickland & Heckman (2009) constrained the wind parameters in the archetypal nearby starburst galaxy M82 using hard X-ray observations of its central region, finding a high thermalization efficiency (~ 1) and a mass-loading efficiency of $\dot{M}_{\text{hot}}/\text{SFR} \sim 0.5$. However, superwinds in other galaxies with star formation rates (SFRs) of $1 - 1000 M_\odot \text{ yr}^{-1}$ at both low and high redshift are much less well studied, and a more generic approach needs to be introduced to constrain the hot wind properties and to understand their dynamical importance for rapidly star-forming galaxies. Therefore, we apply the CC85 model across a wide range of galaxies from dwarf starbursts to ultra-luminous infrared galaxies (ULIRGs). By using the observed X-ray properties of galaxies we constrain the thermalization efficiency and mass loading of hot winds.

Star-forming galaxies are luminous X-ray emitters. In particular, the X-ray luminosities of star-forming galaxies exhibit a tight linear correlation with their SFRs over about four orders of magnitude from $\sim 0.1 M_\odot \text{ yr}^{-1}$ to $\sim 10^3 M_\odot \text{ yr}^{-1}$ (Grimm et al. 2003; Ranalli et al. 2003; Gilfanov et al. 2004; Persic & Rephaeli 2007; Dijkstra et al. 2012; Mineo et al. 2011, 2012a,b, 2014). Observationally, X-ray binaries (XRBs) are the benchmark X-ray tracers that give rise to this linear correlation, but the total X-ray luminosity L_X^{tot} also has contributions from young SN remnants, neutron stars, the warm/hot ISM, and potentially the very hot coronal gas of a CC85-like galactic outflow. The most recent normalization of the linear correlation between the *total* L_X^{tot} and the SFR is

¹ Department of Astronomy, The Ohio State University, 140 W. 18th Ave., Columbus, OH, 43210, USA; dzhang, thompson@astronomy.ohio-state.edu

² Center for Cosmology & Astro-Particle Physics, The Ohio State University, 191 West Woodruff Ave., Columbus, OH, 43210, USA

³ Canadian Institute for Theoretical Astrophysics, 60 St. George Street, University of Toronto, Toronto, ON M5S 3H8, Canada

⁴ Astronomy Department & Theoretical Astrophysics Center, 601 Campbell Hall, University of California, Berkeley, CA 94720, USA

⁵ Canada Research Chair in Astrophysics

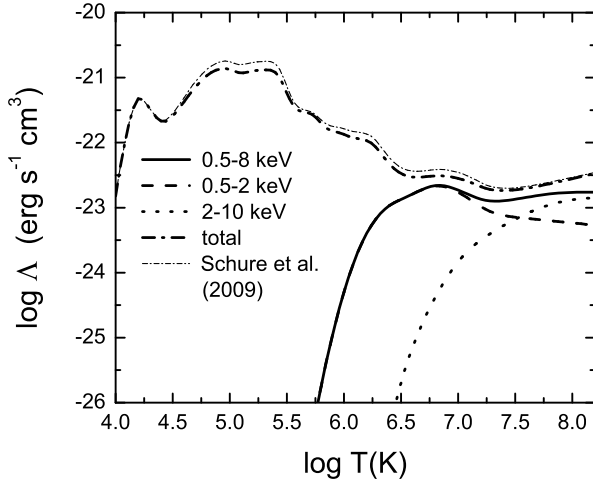


FIG. 1.— Broadband cooling functions calculated by SPEX in different frequency ranges for solar metallicity. The total cooling curve is calculated by integrating the emissivity from 0.1 eV to 1 MeV.

given by Mineo et al. (2014), who find that⁶

$$L_{X(0.5-8\text{keV})}^{\text{tot}}/\text{SFR} \simeq (4.0 \pm 0.4) \times 10^{39} \text{ erg s}^{-1}/(M_{\odot} \text{ yr}^{-1}), \quad (1)$$

where the X-ray emission is from 0.5 keV to 8 keV. Among the multiple contributors to the X-ray emission of galaxies, it is the diffuse emission from hot gas that is of special interest here. As we show in Section 2, considering only X-rays produced by thermal emission, the CC85 model predicts that the diffuse hard X-ray emission from hot wind gas should scale as $L_X \propto \text{SFR}^2$ at fixed thermalization and mass-loading efficiency. Because the observed correlation is $L_X \propto \text{SFR}$ this provides an observational limit on the contribution of hot diffuse X-ray emission, which can then be used to constrain the wind model.

In Section 2 we introduce the CC85 model and calculate the hard X-ray emission from the hot wind fluid. In Section 3 the observed L_X –SFR relation is used to constrain the thermalization and mass-loading efficiency of hot winds. In Section 4 we discuss whether our results change with different parameters in the model and different forms of the observed L_X –SFR correlation. Conclusions are presented in Section 5.

2. SUPERNOVA-DRIVEN HOT WIND MODEL AND EXPECTED X-RAY EMISSION

2.1. The CC85 Galactic Wind Model

The analytic spherically-symmetric hot flow solution derived by CC85 depends on three parameters: the energy input rate \dot{E}_{hot} , mass loss rate \dot{M}_{hot} , and the outflow launch radius R which can be de-dimensionalized either by M82’s parameters (e.g. CC85 model) or the SFR of galaxies (e.g., Strickland & Heckman 2009). For simplicity, two dimensionless parameters α' and β are introduced to normalize the energy input and mass-loading efficiency by

$$\dot{E}_{\text{hot}} = \alpha' \dot{E}_{\text{SN}}, \quad (2)$$

$$\dot{M}_{\text{hot}} = \beta \text{SFR}. \quad (3)$$

⁶ Earlier studies yielded slightly different values of the scalefactor between compact X-ray sources (2–10 keV) and SFR, including (in unit of $\text{erg s}^{-1}/(M_{\odot} \text{ yr}^{-1})$) 0.91×10^{39} (Ranalli et al. 2003), 1.2×10^{39} (Grimm et al. 2003), 2.2×10^{39} (Shtykovskiy & Gilfanov 2005), 0.75×10^{39} (Persic & Rephaeli 2007) and 1.7×10^{39} (Lehmer et al. 2010).

The cumulative net energy input from SNe (\dot{E}_{SN}) is given by

$$\dot{E}_{\text{SN}} = \epsilon \nu \text{SFR}, \quad (4)$$

where $\epsilon = 10^{51} \epsilon_{51}$ ergs is the energy injected by an individual SN, $\text{SFR}_0 = \text{SFR}/(M_{\odot} \text{ yr}^{-1})$, and $\nu = (100M_{\odot})^{-1} \nu_{100}$ is the number of SNe per unit mass of star formation, where typically one SN occurs per $100M_{\odot}$ of stars produced, i.e., $\nu_{100} \simeq 1$. For a Salpeter or Chabrier stellar initial mass function (IMF), $\nu_{100} = 1.18$ and $\nu_{100} = 1.74$, respectively (Leitherer et al. 1999, Strickland & Heckman 2009). Thus we use $\alpha = \alpha' \epsilon_{51} \nu_{100}$ to parameterize the energy injection rate. Here α could in principle be as high as a few, depending on the IMF model, and the contribution to the total heating by stellar winds. We take $\alpha \lesssim 2$ in this paper. Equation (2) is then rewritten as

$$\dot{E}_{\text{hot}} \simeq 3.2 \times 10^{41} \text{ erg s}^{-1} \alpha \text{SFR}_0. \quad (5)$$

The solution to the CC85 model is given in Appendix A. In particular, the temperature T , density n and velocity V_{hot} of the hot wind outflow are

$$T(r) = 6.1 \times 10^7 \text{ K} \mu \left(\frac{\alpha}{\beta} \right) \left[\frac{P_*(r_*)}{\rho_*(r_*)} \right] \quad (6)$$

$$n(r) = 1.4 \text{ cm}^{-3} \alpha^{-1/2} \beta^{3/2} \mu^{-1} R_{200\text{pc}}^{-2} \rho_*(r_*) \text{SFR}_0 \quad (7)$$

$$V_{\text{hot}}(r) = 710 \text{ km s}^{-1} \alpha^{1/2} \beta^{-1/2} u_*(r_*), \quad (8)$$

respectively, where $R_{200\text{pc}} = R/(200 \text{ pc})$, r is the radius of the wind, $r_* = r/R$ is the dimensionless radius, u_* , ρ_* and P_* are the dimensionless velocity, density as functions of dimensionless radius r_* in the CC85 model respectively, and μ is the mean molecular weight. Note that equations (A7) and (A8) in Appendix A show that the density of the hot flow is $n \propto \rho \propto \dot{M}_{\text{hot}}^{3/2} \dot{E}_{\text{hot}}^{-1/2}$. Given fixed α and β , equations (2) and (3) then give $\dot{E}_{\text{hot}} \propto \text{SFR}$ and $\dot{M}_{\text{hot}} \propto \text{SFR}$, thus we have $n \propto \text{SFR}$. For solar abundance $\mu \approx 0.61$, we have $T = 1.5 \times 10^7 \text{ K} (\alpha/\beta)$, $n = 1.1 \text{ cm}^{-3} \alpha^{-1/2} \beta^{3/2} R_{200\text{pc}}^{-2} \rho_*(r=0) \text{SFR}_0$ at the center of the host galaxy ($r = 0$), while $V_{\text{hot}} = 10^3 \text{ km s}^{-1} \alpha^{1/2} \beta^{-1/2}$ at infinity.

2.2. X-ray Cooling and Emission

The diffuse X-ray continuum emission from the hot wind fluid is

$$L_{X,\text{hot}}^{[\nu_1, \nu_2]} = \int n_e n_H \Lambda_N^{[\nu_1, \nu_2]}(T, Z) dV \quad (9)$$

where $\Lambda_N^{[\nu_1, \nu_2]}(T, Z)$ is the emissivity at temperature T , metallicity Z , and in the energy band between two (X-ray) frequencies ν_1 and ν_2 , n_H and n_e are the hydrogen and electron number density respectively. Standard free-free bremsstrahlung emission dominates the cooling rate $\Lambda_N(T, Z)$ for $T \geq 10^7 \text{ K}$ ($\sim 1 \text{ keV}$). A better cooling model should include line emission from ions. Following Schure et al. (2009), we use the SPEX package⁷ (version 2.03.03) to calculate $\Lambda_N(T, Z)$ of a hot plasma in collisional ionization equilibrium (CIE). CIE is a valid assumption if the plasma is dominated by collisional processes and the cooling timescale is longer than the recombination or ionization timescale, otherwise non-equilibrium ionization (NEI) treatments should be taken into account. Strickland & Heckman (2009) found that it is justified to use CIE treatment in M82, and Schure et al. (2009) discussed that the differences between NEI and CIE emission are quite small

⁷ <http://www.sron.nl/spex>

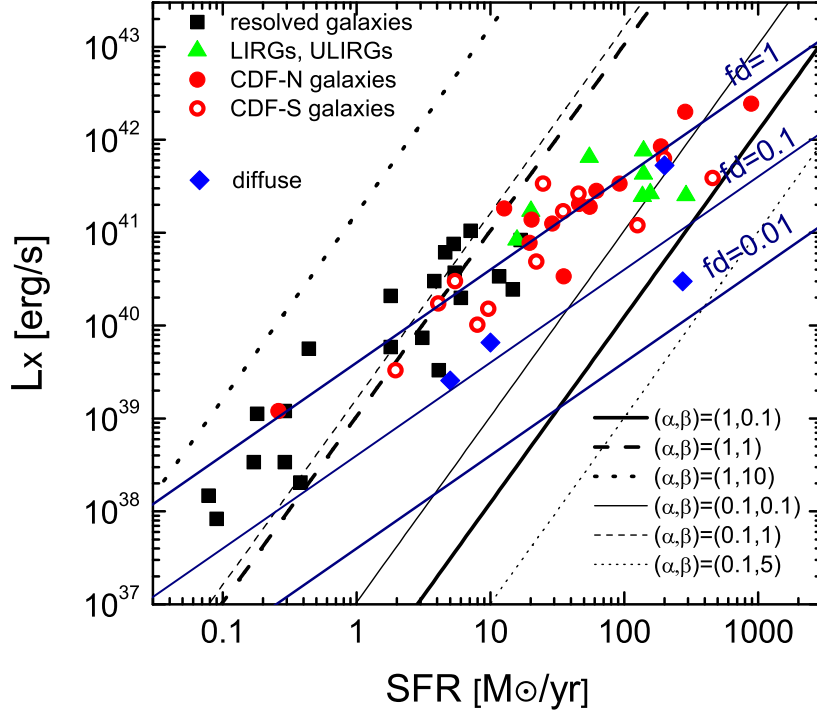


FIG. 2.— X-ray luminosity L_X of the hot wind at 0.5–8 keV ($L_{X,\text{hot}}$) with the set of parameters $(\alpha, \beta) = (1, 0.1), (1, 1), (1, 10)$ (thick lines) and $(0.1, 0.1), (0.1, 1), (0.1, 10)$ (thin lines) and assuming $R = 200$ pc, compared with the diffuse X-ray luminosity ($L_{X,\text{diffuse}}$) from galaxies where the fraction of diffuse X-ray emission $f_d = 0.01, 0.1$ or 1 (blue lines). Black squares, green triangles, and red circles are the total X-ray luminosities of resolved galaxies, LIRGs, ULIRGs, *Chandra Deep Field North* (CDF-N) and *Chandra Deep Field South* (CDF-S) galaxies in Mineo et al. (2014). The four blue diamonds are the diffuse X-rays (not total) from M82, NGC 253, NGC 6240 and Arp 220 (see Section 4).

for $T \geq 10^6$ K. Therefore we adopt CIE treatment. Figure 1 shows the 0.5–8 keV, 0.5–2 keV, 2–10 keV, and the total cooling functions by integrating over the energy range from 0.1 eV to 1 MeV. Solar abundances from Lodders et al. (2009) are assumed in this calculation, thus the total cooling function is slightly different from Schure et al. (2009) who adopted solar abundances from Anders & Grevesse (1989). The total cooling curve has an order of $\Lambda_N \sim 10^{-22.5}$ erg s $^{-1}$ cm 3 for $T \geq 10^6$ K, while the cooling functions at 0.5–8 keV and 0.5–2 keV reach maximum $\simeq 10^{-22.7}$ erg s $^{-1}$ cm 3 at $T \simeq 10^{6.8}$ K.

The densities n_H can be calculated using CC85 model equation (7), assuming the mass fraction of hydrogen for solar abundances $X_H \approx 0.71$. The ionization fraction n_e/n_H is also calculated by SPEX (Schure et al. 2009). Thus, the total X-ray luminosity between two frequencies ν_1 and ν_2 is written as

$$L_{X,\text{hot}}^{[\nu_1, \nu_2]} \approx 1.5 \times 10^8 L_\odot X_H^2 \left(\frac{\beta^3 \text{SFR}_0^2}{\alpha R_{200\text{pc}}^2} \right) \times \int_0^\infty dr_* r_*^2 \rho_*^2 \Lambda_{N,-22}^{[\nu_1, \nu_2]} \left(\frac{n_e}{n} \right), \quad (10)$$

where $\Lambda_{N,-22}^{[\nu_1, \nu_2]} = \Lambda_N^{[\nu_1, \nu_2]} / 10^{-22}$ erg s $^{-1}$ cm 3 , other variables are denoted in Section 2.1. Note the scaling of $L_{X,\text{hot}}$ with SFR, and that equation (7) gives $n \propto \text{SFR}$. Thus equation (10) shows that X-ray emission from the hot wind fluid scales as

$$L_{X,\text{hot}} \propto n^2 \Lambda_N \propto \text{SFR}^2, \quad (11)$$

significantly steeper than the observed linear relation $L_X \propto \text{SFR}$ for star-forming galaxies.

3. THE OBSERVED L_X –SFR RELATION CONSTRAINS HOT WINDS

In this paper we focus on the diffuse X-ray emission from the hot wind fluid. Because the fraction of the observed hard X-ray emission that is actually due to diffuse gas rather than other sources is uncertain, we adopt the following relation between the diffuse emission at 0.5–8 keV and SFR based on the discussion in Section 1:

$$L_{X,\text{diffuse}}(0.5\text{--}8\text{ keV}) = 4.0 \times 10^{39} f_d \text{ erg s}^{-1} \text{SFR} / (M_\odot \text{ yr}^{-1}), \quad (12)$$

where $f_d \leq 1$ is the fraction of the diffuse emission in X-rays due to the hot wind fluid, and $f_d = 1$ is the observed mean relation between total X-ray emission and SFR. In general, we expect $f_d \sim 0.1$, as seen in M82 (Strickland & Heckman 2009), but higher and lower values are considered throughout this paper. In Section 4 we discuss constraints on f_d based on some well-studied starbursts. Theoretical constraints on the hot wind fluid from the observed diffuse X-ray emission can then be obtained by combining equations (10) and (12) such that

$$L_{X,\text{hot}} = L_{X,\text{diffuse}}, \quad (13)$$

where the hard X-ray emission is from 0.5 keV to 8 keV (i.e., $\nu_1 = 0.5$ keV and $\nu_2 = 8$ keV in equation [10] and Fig. 1).

There are five parameters in equation (13): α , β , SFR, R , and f_d . Using equation (13), the relation between any two of the five parameters can be constrained by the other three parameters. However, the constraints on the CC85 model, in

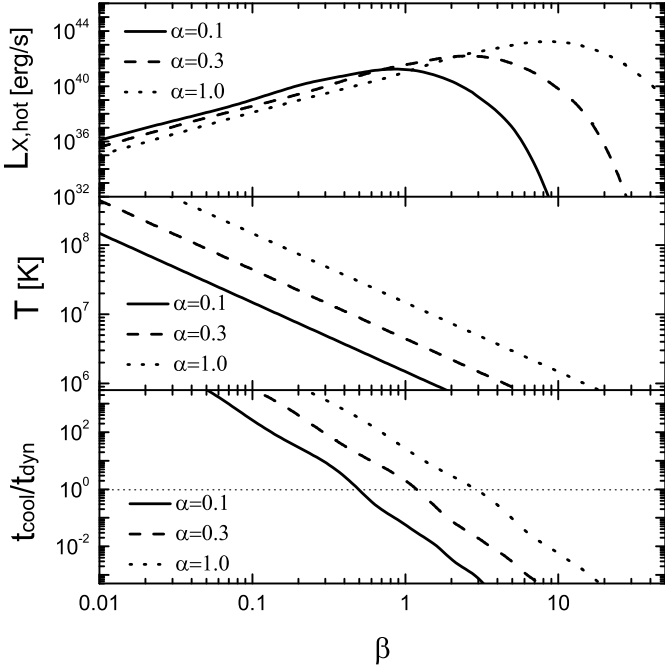


FIG. 3.— Total hot X-ray luminosity $L_{X,\text{hot}}$ between 0.5–8 keV (upper), galactic center temperature $T(r=0)$ (middle) and the ratio of the cooling and dynamic timescale $t_{\text{cool}}/t_{\text{dyn}}(r=R)$ (lower) as a function of β for fixed α . The wind launching radius $R = 200$ pc and $\text{SFR} = 10 M_{\odot} \text{ yr}^{-1}$.

particular, the parameter set of (α, β) are of particular interest, since α and β determine the importance of the hot gas for driving matter out of the galaxy directly, and for driving swept up cold gas clouds out of the galaxy via ram pressure. If we fix f_d in equation (13), with a fixed R (or apply an independent model of $R(\text{SFR})$), we can solve for the relation between α , β , and SFR.

Figure 2 shows X-ray luminosities $L_{X,\text{hot}}$ as a function of SFR with some given values of (α, β) (black lines), compared with the diffuse luminosity $L_{X,\text{diffuse}}$ with different f_d (blue lines). The radius R is fixed at $R = 200$ pc for illustrative purposes. Other values of R give similar results. The slope of $L_{X,\text{hot}}$ is steeper than $L_{X,\text{diffuse}}$, due to the different scaling between bremsstrahlung emission from the hot wind $L_{X,\text{hot}} \propto \text{SFR}^2$, and the observed X-ray luminosity $L_X \propto \text{SFR}$ (equations [10] and [12]). Each point of intersection between two lines $L_{X,\text{hot}}$ and $L_{X,\text{diffuse}}$ for any value of f_d gives a certain parameter set of α , β and SFR. For example, for $f_d = 0.1$ and $(\alpha, \beta) = (1, 1)$, Figure 2 shows that $L_{X,\text{hot}}$ intersects $L_{X,\text{diffuse}}$ at $\text{SFR} \sim 0.4 M_{\odot} \text{ yr}^{-1}$, implying that for $f_d = 0.1$, $(\alpha, \beta) = (1, 1)$ is only allowed for galaxies with $\text{SFR} \lesssim 0.4 M_{\odot} \text{ yr}^{-1}$; for $\text{SFR} \gtrsim 0.4 M_{\odot} \text{ yr}^{-1}$, $(\alpha, \beta) = (1, 1)$ produces too much diffuse X-ray emission. Similarly, note that $(\alpha, \beta) = (1, 10)$ is completely ruled out because it always produces too much diffuse X-ray emission. One might expect that in general higher values of β (i.e., larger mass loading) would always lead to higher diffuse X-ray luminosity and tighter constraints on the allowed range of SFR, but the $L_{X,\text{hot}}$ lines for $\alpha = 0.1$ (thin lines) show that this is not the case. In fact, $L_{X,\text{diffuse}}$ for $(\alpha, \beta) = (0.1, 5)$ falls below other lines with lower $\beta = 0.1$ and 1, this is because the temperature of the flow for $(\alpha, \beta) = (0.1, 5)$ is so cool that only a small amount

of the emission from the wind fluid is in the X-ray band. In fact, multiple solutions for β exist at fixed α and SFR. For example, for $f_d = 0.1$ and $\alpha = 0.1$, both $\beta \simeq 0.1$, and $\beta \sim 1$ are valid solutions in the CC85 model for $\text{SFR} = 10 M_{\odot} \text{ yr}^{-1}$.

Figure 3 makes the solutions for β more explicit. For fixed α , $L_{X,\text{hot}}$ in equation (10) has a maximum as a function of β . The top panel of Figure 3 shows that $L_{X,\text{hot}}$ is thereby peaked as a function of β . For a given $L_{X,\text{hot}}$ below the peak, there are two solutions for β , one low, and another high. As shown in the middle panel of Figure 3, the low value of β corresponds to high T , and high β to low T . However, not all solutions of β are physically realizable in the CC85 model, because of radiative cooling. The CC85 model assumes that the flow is adiabatic for $r > R$ and fluid cooling is not important throughout the wind profile. If the cooling timescale in a mass loaded wind t_{cool} becomes smaller than the local dynamical timescale $t_{\text{dyn}} \sim r/V_{\text{hot}}$, then this assumption is invalidated and the CC85 model must break down. The wind dynamical timescale is

$$t_{\text{dyn}} \sim 2.8 \times 10^5 \text{ yr } \alpha^{-1/2} \beta^{1/2} u_*^{-1} R_{200\text{pc}} \left(\frac{r}{R}\right). \quad (14)$$

The total energy is $\varepsilon_{\text{heat}} = \rho \left(\frac{1}{2} V_{\text{hot}}^2 + \frac{c_s^2}{\gamma-1} \right) = \rho_* \dot{E}^{1/2} \dot{M}^{1/2} / R^2$, thus the cooling timescale is estimated by $t_{\text{cool}} \sim \varepsilon_{\text{heat}} / (n_e n_{\text{H}} \Lambda_{\text{N}})$. Note that the ratio of $t_{\text{cool}}/t_{\text{dyn}}$ of the hot wind has its lowest value at $r = R$; thus we can focus on $t_{\text{cool}}/t_{\text{dyn}}$ at $r = R$ as the strongest timescale constraint. If we take bremsstrahlung emission from the pure hydrogen gas as a lower limit for the cooling rate Λ_{N} , we obtain an analytic upper bound on β :

$$\beta \leq 6.6 \alpha^{3/5} R_{200\text{pc}}^{2/5} \left(\frac{10 M_{\odot} \text{ yr}^{-1}}{\text{SFR}} \right)^{2/5} \left(\frac{\Lambda_{\text{brems}}^{\text{H}}}{\Lambda_{\text{N}}} \right)^{2/5}. \quad (15)$$

The lower panel of Figure 3 shows the numerical results for $t_{\text{cool}}/t_{\text{dyn}}$ at $r = R$, which decreases strongly with increasing β . Since $t_{\text{cool}} < t_{\text{dyn}}$ at high β , these high- β solutions are not physical in CC85 adiabatic wind model.

Figure 4 shows both the solution for β from equation (13) as a function of SFR, and constraints from radiative cooling. The thick lines in each panel are solutions for fixed $f_d = 0.1$ for two different models of R : $R = 200$ pc and $R \propto \text{SFR}^{1/2}$ (Heckman et al. 2000; see also Lehnert & Heckman 1996, Meurer et al. 1997, Martin 2005), and fixed $\alpha = 1$ (left panel) and 0.1 (right panel). The thin solid and dashed lines show the critical condition $t_{\text{cool}} = t_{\text{dyn}}$ at $r = R$ from equation (15), where we have used the total emissivity Λ_{N} from Figure 1. Above the line $t_{\text{cool}} < t_{\text{dyn}}$, the wind is radiative outside the host galaxy, and the CC85 model breaks down. For $\alpha = 0.1$, there are two solutions for β , but the high- β solutions are excluded by the radiative cooling constraint (equation [15]). Below the solution curves $f_d < 0.1$, and above these curves $f_d > 0.1$. Importantly, one finds that compact rapidly star-forming galaxies should in general have relatively low β . Taking $\alpha = 1$ and $R = 200$ pc, we see that for $\text{SFR} \gtrsim 10 M_{\odot} \text{ yr}^{-1}$ that $\beta \lesssim 0.3$. For lower $\alpha = 0.1$, the limit on β decreases to $\beta \lesssim 0.15$. Thus, it does not appear possible for the CC85 alone to account for $\beta \sim 1-10$, as seems to be required in galaxy formation models (Springel & Hernquist 2003; Oppenheimer & Davé 2006, 2008; Finlator & Davé 2008; Bower et al. 2012; Puchwein & Springel 2013). For example, Puchwein & Springel (2013) (see also Bower et al. 2012) shows that $\beta \sim 1-10$ is required to match the observed galaxy stellar mass function. Note that for lower assumed values of α or f_d all of the solution curves move down in β , making the limits on β even stronger.

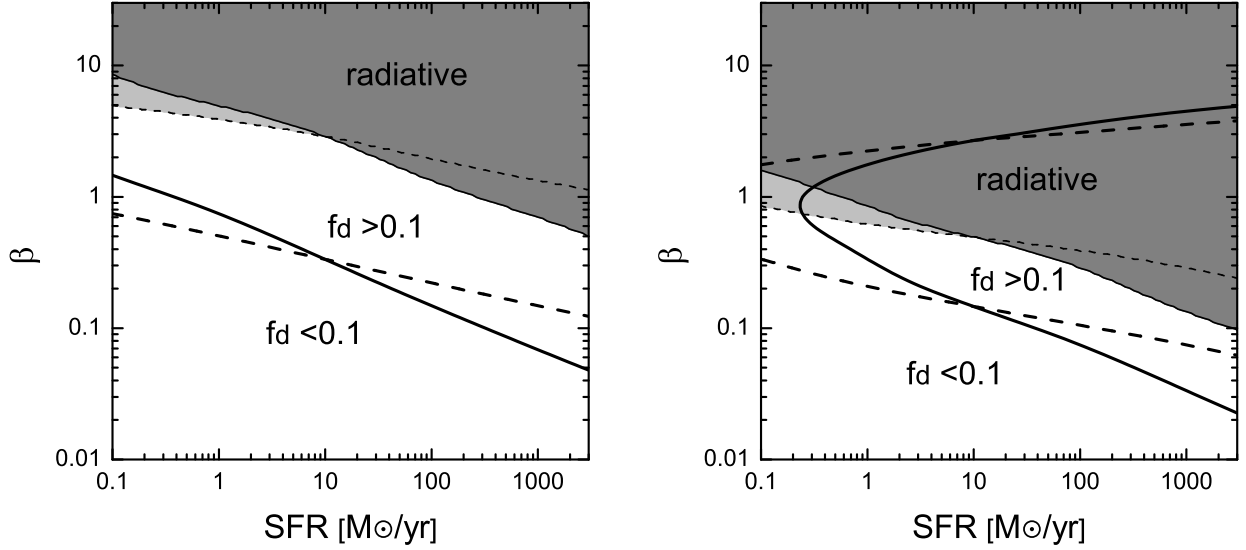


FIG. 4.— Solutions of β as a function of SFR for fixed $\alpha = 1$ (left panel) and $\alpha = 0.1$ (right panel), with $f_d = 0.1$, and the wind launching radius $R = 200$ pc (solid lines), $R = 200$ $(\text{SFR}/\text{SFR}_n)^{1/2}$ pc (dashed lines) with the normalization $\text{SFR}_n = 10 M_\odot \text{yr}^{-1}$ (dotted lines). The gray regions give where the flow is radiative $t_{\text{dyn}} \geq t_{\text{cool}}$ at $r = R$.

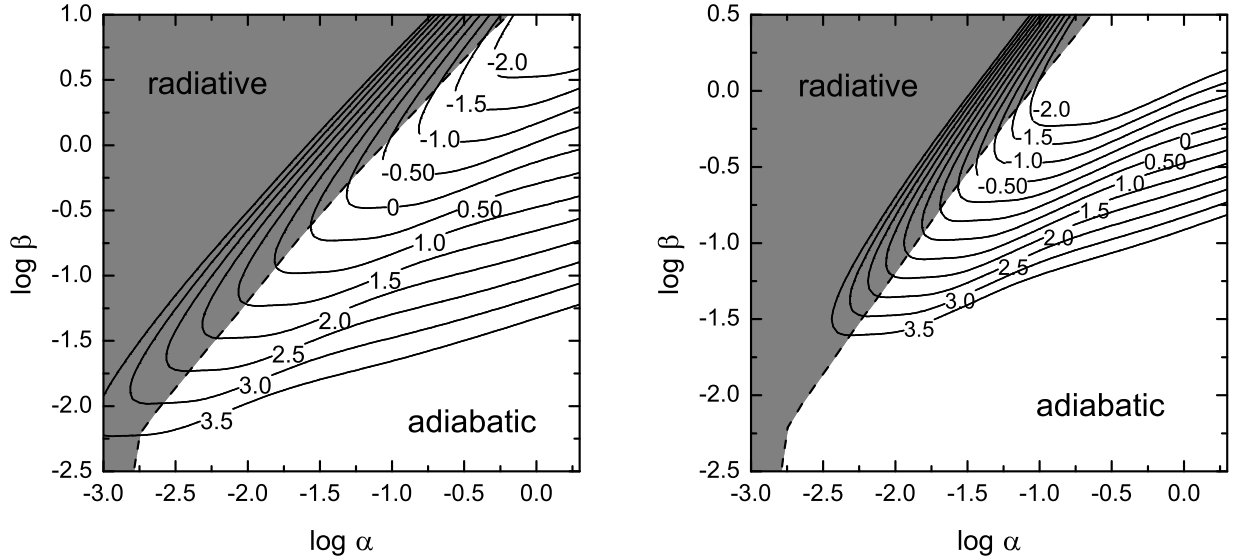


FIG. 5.— Contours of solutions of SFR $\log_{10}(\text{SFR}/M_\odot \text{yr}^{-1})$ as a function of (α, β) by equation (13), with $f_d = 0.1$ and $R = 200$ pc (left) and $R = 200$ $(\text{SFR}/\text{SFR}_n)^{1/2}$ with $\text{SFR}_n = 10 M_\odot \text{yr}^{-1}$ (right). The dashed line is the critical line $t_{\text{dyn}} = t_{\text{cool}}$ at $r = R$ based on equation (16).

Constraints on β for a broader range of α are shown in the $\alpha - \beta$ plane in Figure 5, which shows contours of solutions of $\log_{10}(\text{SFR}/M_\odot \text{yr}^{-1})$ by equation (13), with fixed $f_d = 0.1$, and $R = 200$ pc and $R \propto \text{SFR}^{1/2}$. For example, taking $\text{SFR} = 10 M_\odot \text{yr}^{-1}$, we see that $\beta \lesssim 0.3$ for $\alpha = 1$ and $\beta \lesssim 0.06$ for $\alpha = 0.01$. Also, we find that larger R yields a smaller allowed (α, β) space for the same SFRs. Note that the cooling constraint equation (15) is independent of equation (13). Combining equations (13) and (15) by solving SFR by equation (13) as a function of α , β , R and f_d , the cooling constraint becomes a function of f_d . Thus $t_{\text{cool}}/t_{\text{dyn}}(r = R) \geq 1$ takes the form

$$6.3 \times 10^3 \alpha \Lambda_{N,-22}^{-1} f_d^{-1} \left(\frac{n_e}{n_H} \right)^{-1}$$

$$\times \int_0^\infty dr_* r_*^2 \rho_*^2 \Lambda_{N,-22}^{[\nu_1, \nu_2]} \left(\frac{n_e}{n_H} \right) \geq 1, \quad (16)$$

which is independent of R . The grey region above the thick solid diagonal line ($t_{\text{cool}} = t_{\text{dyn}}$ at $r = R$) in Figure 5 denotes radiative winds excluded by equation (16). The allowed values of β are seen to decrease rapidly for lower α and SFR at fixed f_d .

Finally, we note that Chevalier & Clegg (1985) ignored the effect of gravity, because they focused on solutions for M82 with $\alpha \approx \beta$, and thus they derived a terminal velocity of the M82 outflow of $V_{\text{term}} \simeq 1000 \text{ km s}^{-1}$, much higher than the escape velocity from the galaxy V_{esc} of a few hundred km s^{-1} (Greco et al. 2012). If we consider the general constraint that

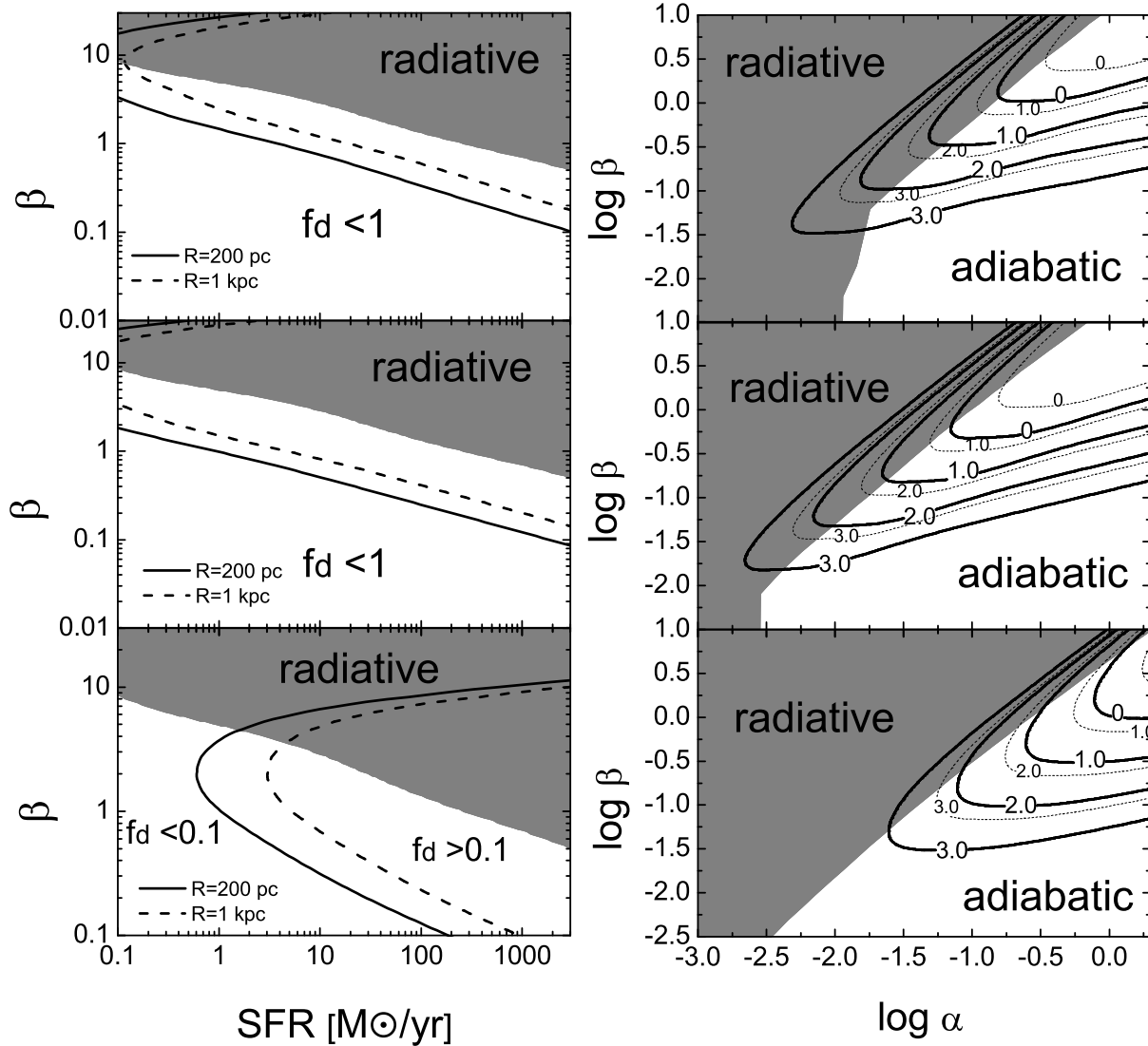


FIG. 6.— Solutions for β as a function of SFR for fixed $\alpha = 1$ (left panels) and contours of SFR $\log_{10}(\text{SFR}/M_{\odot} \text{ yr}^{-1})$ as a function of α and β (right panels) for different R : $R = 200$ pc (solid lines) and 1 kpc (dashed lines). The gray radiative regions in left panels are excluded by equation (15) with $R = 200$ pc, while in right panels the gray radiative regions are excluded by equation (16) with the corresponding f_d mentioned below. The upper panels show the results based on the soft X-ray L_X –SFR relation using equation (12) with $f_d = 1$, the middle panels are based on L_X –SFR relation in Mineo et al. (2012b) with $f_d = 1$, and the lower panels are based on the hard X-ray L_X –SFR relation in Lehmer et al. (2010) with $f_d = 0.1$.

requires $V_{\text{term}} > V_{\text{esc}}$ for an unbound outflow we find that

$$\beta < \alpha \left(\frac{V_{\text{esc}}}{1000 \text{ km s}^{-1}} \right)^{-2}. \quad (17)$$

For $V_{\text{esc}} = 200 \text{ km s}^{-1}$, this criterion is not restrictive, but for deep gravitational potentials ($V_{\text{esc}} \gtrsim 400 \text{ km s}^{-1}$), this limit on β becomes close to the constraints produced by the critical lines of $t_{\text{cool}} = t_{\text{dyn}}$ in Figures 4 and 5.

4. DISCUSSION

There are several parameters in our model for the diffuse X-ray emission associated with galactic winds, including the diffuse fraction f_d , the normalization factor for the observed

L_X –SFR correlation, and the selected X-ray energy range. It is important to investigate whether our constraints on α and β change with changing parameters in the model.

Constraints on f_d can also be given by some well-studied starbursts with diffuse X-ray data, such as M82, NGC 253, NGC 6240 and Arp 220. We use equation (12) to calculate f_d . Figure 2 shows the diffuse X-ray emission from these galaxies in blue diamonds. The observed extended X-ray luminosity in M82 from 0.1 to 2.4 keV band is $L_X^{0.1-2.4\text{keV}} \sim 1.9 \times 10^{40} \text{ erg s}^{-1}$ (Strickland et al. 1997), and in the 2-8 keV band is $L_X^{2-8\text{keV}} \leq 4.4 \times 10^{39} \text{ erg s}^{-1}$ (Strickland & Heckman 2007). The total 8-1000 μm infrared luminosity of M82 $L_{\text{IR}} \simeq 5.6 \times 10^{10} L_{\odot}$

(Sanders et al. 2003) corresponds to a SFR of $\sim 5 - 10 M_\odot \text{ yr}^{-1}$ (O’Connell & Manganano 1978; Kennicutt 1998; Förster Schreiber et al. 2003; Strickland et al. 2004; Elbaz et al. 2007; Strickland & Heckman 2009; Panuzzo et al. 2010), depending on the assumed IMF. If we convert the observed diffuse X-ray from 2–8 keV to 0.5–8 keV with a conversion factor of 1.5, as assumed in Mineo et al. (2012a), we get the diffuse fraction $f_d \lesssim 0.16$ for the upper bound of SFR as $10 M_\odot \text{ yr}^{-1}$, and $f_d \lesssim 0.32$ for a lower estimated SFR = $5 M_\odot \text{ yr}^{-1}$. Another starburst with diffuse X-ray data is NGC 253, which has an unabsorbed 2–10 keV luminosity of $2 \times 10^{39} \text{ erg s}^{-1}$ (Weaver et al. 2002). Taking the total SFR of NGC 253 as $5 M_\odot \text{ yr}^{-1}$ (Melo et al. 2002), we get $f_d \sim 0.13$. NGC 6240, however, has been recently observed with a high diffuse luminosity $5.3 \times 10^{41} \text{ erg s}^{-1}$ at 0.5–8 keV (Wang et al. 2013), which indicates a high value of $f_d \simeq 1.3$ for a total SFR of $\sim 100 M_\odot \text{ yr}^{-1}$ (Heckman et al. 2000). A higher estimated SFR of $\sim 200 M_\odot \text{ yr}^{-1}$ gives $f_d \sim 0.7$. McDowell et al. (2003) observed individual sources of extended X-ray emission in Arp 220. Following their suggestion that the inner two plumes of hot gas with a luminosity of $\sim 3 \times 10^{40} \text{ erg s}^{-1}$ are due to a galactic wind, we get $f_d \sim 0.03$ for Arp 220. In short, the nearby well-studied starbursts show that in general it is reasonable to take $f_d \lesssim 0.1$ as the typical value for the diffuse X-ray emission. However, for some galaxies, such as NGC 6240, $f_d \sim 1$ is also possible. The upper panels in Figure 6 shows solutions for β using equations (13) and the L_X –SFR relation (eq. [12]), but for $f_d = 1$, $R = 200 \text{ pc}$ and 1 kpc . Compared with Figures 4 and 5 (left panels), higher f_d or larger R do not change our results qualitatively. For example, for $\alpha = 1$ we still find $\beta \lesssim 1$ for SFR $\gtrsim 10 M_\odot \text{ yr}^{-1}$.

We also check whether different normalizations of L_X –SFR based on a different SFR estimate or energy range change our results. For example, Mineo et al. (2012b) studied the soft X-ray luminosity of the diffuse ISM and obtained the linear relation

$$L_{X(0.5-2)\text{keV}}^{\text{tot}}/\text{SFR} \simeq (8.3 \pm 0.1) \times 10^{38} \text{ erg s}^{-1}/(M_\odot \text{ yr}^{-1}), \quad (18)$$

over the range of SFRs from ~ 0.1 to $\sim 17 M_\odot \text{ yr}^{-1}$. Assuming equation (18) holds for all SFRs, the middle panels of Figure 6 give constraints on β with a maximum $f_d = 1$, which assumes all soft X-rays are from the diffuse component. As another example, we adopt the hard X-ray L_X –SFR scaling by Lehmer et al. (2010) (their Table 4, Model 1)

$$L_{X(2-10)\text{keV}}^{\text{tot}}/\text{SFR} \simeq 10^{39.24 \pm 0.06} \text{ erg s}^{-1}/(M_\odot \text{ yr}^{-1}). \quad (19)$$

Taking the typical value $f_d = 0.1$, the lower panels in Figure 6 show the results using Equation (19) with $R = 200 \text{ pc}$ and 1 kpc . In general, for $\alpha = 1$, we always find that $\beta \lesssim 1$ for SFR $> 10 M_\odot \text{ yr}^{-1}$, with an uncertainty of a factor of a few for different L_X –SFR normalizations, and adopted values of f_d and R . The middle and lower contour panels in Figure 6 show that the hard X-ray constraint is weaker than the soft X-ray constraints from equation (18), but our basic conclusion that large β is excluded in the CC85 model is not changed qualitatively.

It is worthwhile to highlight the limitations of the CC85 model. Note that the breakdown of the adiabatic CC85 model at large β as a result of radiative cooling highlighted in Section 3 is consistent with Silich et al. (2003, 2004), who showed that an adiabatic stationary solution of the wind does not exist with \dot{E}_{hot} or \dot{M}_{hot} larger than a critical value.

Too large \dot{M}_{hot} produces a so-called bimodal solution of the flow (e.g., Tenorio-Tagle et al. 2007; Wunsch et al. 2008; Wunsch et al. 2011), in which the densest inner regions immediately radiate away the deposited energy while the outer zones develop a strongly radiative wind. We compute the ratio of $n_e n_H \Lambda_N / q_{\text{hot}}$, where $q_{\text{hot}} = 3\dot{E}_{\text{hot}}/(4\pi R^3)$ is the volumetric heating rate inside the galaxy. Since $n_e n_H \Lambda_N / q_{\text{hot}}$ decreases as a function of radius inside the galaxy, we focus on the ratio $n_e n_H \Lambda_N / q_{\text{hot}}$ at the center of the host galaxy ($r = 0$). If $n_e n_H \Lambda_N / q_{\text{hot}} > 1$ at the center, the hot fluid becomes radiative and unstable as discussed by Silich et al. (2004) and their series of papers, and again the assumptions of the CC85 model break down. Although the thick solid line in Figure 5 corresponds to $t_{\text{cool}} = t_{\text{dyn}}$, we find that it gives a similar bound to $n_e n_H \Lambda_N = q_e$ at $r = 0$, so that for β above this line we expect an unstable and radiative hot fluid inside the galaxy.

Moreover, the CC85 model also has some other simplifications. In particular, it assumes spherical symmetry and radius-independent energy thermalization and mass-loading efficiency densities (i.e., constant q and Q in the CC85 model, see Appendix A). The issue of spherical symmetry has been addressed by Strickland & Heckman (2009), who find that it is possible to use the spherical analytical CC85 model to predict the wind fluid properties and X-ray emission from a disklike starburst for M82-like systems. Similarly, one might imagine that a more realistic volumetric energy thermalization and mass-loading efficiency densities that are functions of radius would change the properties of the wind solutions and call our results into question. For simplicity if we assume a radius-dependent energy and mass injection density $Q \propto r^{-\xi}$ and $q \propto r^{-\xi}$ in the CC85 model, the solutions of the hot wind (u_* , ρ_* and P_*) change inside the galaxy $r < R$ (see equations [A13], [A14] and [A15] in Appendix A as the solutions). For example, the Mach number of the wind becomes $M \approx \sqrt{(\xi-1)/[\gamma(3-\xi)]}$ at $r \ll R$ for $1 < \xi < 3$, which is different from the case of $\xi < 1$ that $M \approx 0$ at $r \ll R$. For the purpose of this paper we focus on integrated constraints α and β given by equations (3) and (5). For example, we find that for $\alpha = 1$, the constraint on β for SFR $\gtrsim 1 M_\odot \text{ yr}^{-1}$ changes by less than a factor of 50% as a function of ξ in the range of $0 \leq \xi < 3$. For a wide range of $\alpha \lesssim 2$, the basic conclusion in this paper that $\beta \lesssim 1$ for SFR $\gtrsim 10 M_\odot \text{ yr}^{-1}$ in the CC85 model still holds. Of course real galaxies are clumpy, with a complex ISM. It is worthwhile to study the effects of multiphase and clumpy nature of wind on the dynamics and X-ray emission of the wind. Some hydrodynamical simulations with more realistic and complex wind structure (e.g., Cooper et al. 2008, 2009; Fujita et al. 2009, Hopkins et al. 2012) showed comparisons between X-ray emission in the model and observations, as well as estimate on mass-loading efficiency. However, these works are mostly applied for M82-like and dwarf starbursts. More detailed X-ray comparisons between models and observations should be done for starburst galaxies across a wide range of SFRs in the future.

5. CONCLUSIONS

In this paper we constrain the properties of any potential hot galactic wind from galaxies varying from dwarf starbursts to ULIRGs using the adiabatic hot wind model of Chevalier & Clegg (1985). Numerical simulations have shown that this model provides a good description of the hot wind fluid (e.g., Strickland & Heckman 2009). We use the observed total X-ray luminosities of galaxies to constrain the efficiency α (i.e., energy input rate; eq. 3) and the mass-loading

efficiency β (eq. 5) of the hot wind. We first showed that the diffuse hard X-ray luminosity from any putative hot outflow should scale as $L_{X,\text{hot}} \propto \text{SFR}^2$ for fixed α and β (eq. 10). However, observations show a linear relation between the total galactic X-ray luminosity and SFR (Fig. 2). If we attribute a fraction ($f_d < 1$) of this total emission to the hot wind fluid we derive constraints on α and β as a function of SFR and the wind launching radius R (Figs. 4 and 5). We showed that for fixed f_d there exist multiple solutions for β (one low and one high) as a function of α and SFR (Fig. 3). We highlight the importance of radiative cooling for the heavily mass-loaded high- β solutions, which invalidates the adiabatic CC85 model (eq. 15). The breakdown of the CC85 model at large β is consistent with Silich et al. (2003, 2004), who showed that the adiabatic stationary solution of the wind does not exist with \dot{E}_{hot} or \dot{M}_{hot} larger than a critical value. As a result, we showed that only moderate mass-loading is allowed in the CC85 model. For example, as Figure 5 gives, for reasonable values of the thermalization efficiency $\alpha \lesssim 1$, and for $\text{SFR} \gtrsim 10 M_\odot \text{ yr}^{-1}$ we find that $\beta \lesssim 1$; higher values of β would require that significantly more of the total X-ray luminosity of star-forming galaxies be attributable to the hot flow, in conflict with observations that find that the X-ray luminosities of galaxies are dominated by compact objects. These conclusions do not change for reasonable variations about our fiducial model (Fig. 6).

Our result that $\beta \lesssim 1$ for $\text{SFR} \gtrsim 10 M_\odot \text{ yr}^{-1}$ shows that it does not appear possible for an adiabatic CC85 model alone to account for $\beta \sim 1 - 10$ as seems to be required by integrated constraints on the efficiency of stellar feedback in galaxies (Springel & Hernquist 2003; Oppenheimer & Davé 2006, 2008; Finlator & Davé 2008; Bower et al. 2012; Puchwein & Springel 2013). For example, Puchwein & Springel (2013) (see also Bower et al. 2012) show that $\beta \sim 1 - 10$ is required to match the observed galaxy stellar mass function. However, it remains possible that the swept up cold gas carries most of the mass (e.g., Cooper et al. 2008, 2009; Fujita et al. 2009), or that other wind driving mechanisms such as momentum deposition by supernovae and radiation pressure on dust (Murray et al. 2005) or cosmic rays (Everett et al. 2008; Socrates et al. 2008) dominate wind driving.

Finally, there are several additional studies that can further constrain and explain hot winds. First, since the CC85 model assumes a radius-independent energy input and mass-loading efficiency densities in the wind, it is worthwhile to investigate the effects of multiphase and clumpy nature of winds on their dynamics and X-ray emission across a wide range of galactic SFRs. We encourage more detailed multi-dimensional simulations like those of Cooper et al. (2008, 2009), Fujita et al. (2009) and Hopkins et al. (2012), but for massive starbursts like Arp220 and other ULIRGs to assess their integrated X-ray emission for comparison with observations. Second, the inclusion of a model of cold cloud acceleration and destruction in the CC85 model may further constrain the hot wind model. Note that a traditional way to explain the cold gas in galactic winds is that the cold gas clouds enter the SN-heated hot wind flow at relatively low velocity and are accelerated by the ram pressure of the hot wind. In a future work, we will combine a model of cold cloud acceleration and destruction with the CC85 model to constrain energy thermalization and hot-wind mass-loading efficiency in individual systems that have measured cold cloud velocities, incorporating the constraints on the hot wind determined in this paper. Lastly, it is clear that radiative cooling is important for the dynamics of outflows across a wide range of parameter space of thermalization input and high mass-loading efficiency. Formulating radiative solutions for high- β winds and comparing with observations is an important direction for future work.

6. ACKNOWLEDGEMENTS

We thank the anonymous referee for comments that have allowed us to improve our paper. D.Z. and T.A.T. thank Smita Mathur and David Weinberg for helpful discussions on the cooling functions of X-ray emission and wind mechanisms. T.A.T. also thanks Tim Heckman for a number of stimulating discussions. This work is supported in part by NASA grant # NNX10AD01G. E.Q. is supported in part by NASA ATP Grant 12-ATP12-0183, a Simons Investigator award from the Simons Foundation, the David and Lucile Packard Foundation, and the Thomas Alison Schneider Chair in Physics. N.M. is supported in part by NSERC of Canada and by the Canada Research Chair program.

APPENDIX

A. CC85 MODEL

CC85 present a spherical thermal winds where gravitational forces can be ignored. Assuming inside the radius of the starburst region R the total mass and energy input are \dot{M}_{hot} and \dot{E}_{hot} respectively, with an averaged injected efficiencies per unit volume in the galaxy being $q = \dot{M}_{\text{hot}}/V$, $Q = \dot{E}_{\text{hot}}/V$ and $V = 4\pi R^3/3$. The one-dimensional hydrodynamic equations for the hot fluid are

$$\frac{1}{r^2} \frac{d}{dr} (\rho u r^2) = q \quad (\text{A1})$$

$$\rho u \frac{du}{dr} = -\frac{dP}{dr} - qu \quad (\text{A2})$$

$$\frac{1}{r^2} \frac{d}{dr} \left[\rho u r^2 \left(\frac{1}{2} u^2 + \frac{\gamma}{\gamma-1} \frac{P}{\rho} \right) \right] = Q. \quad (\text{A3})$$

The solutions for the Mach number M of the hot wind fluid are given in CC85 by (see also Cantó et al. 2000)

$$\left[\frac{(\gamma-1) + 2/M^2}{\gamma+1} \right]^{(1+\gamma)/[2(1+5\gamma)]} \left[\frac{3\gamma+1/M^2}{1+3\gamma} \right]^{-(3\gamma+1)/(5\gamma+1)} = \frac{r}{R}, \quad (\text{A4})$$

for $r < R$ and

$$M^{2/(\gamma-1)} \left(\frac{\gamma-1+2/M^2}{1+\gamma} \right)^{(\gamma+1)/[2(\gamma-1)]} = \left(\frac{r}{R} \right)^2. \quad (\text{A5})$$

for $r > R$. We take the dimensionless variables as

$$P = P_* \dot{M}^{1/2} \dot{E}^{1/2} R^{-2} \quad (\text{A6})$$

$$\rho = \rho_* \dot{M}^{3/2} \dot{E}^{-1/2} R^{-2} \quad (\text{A7})$$

$$u = u_* \dot{M}^{-1/2} \dot{E}^{1/2}. \quad (\text{A8})$$

Thus these variables can be calculated by

$$u_*^2 = 2M^2 / \left(M^2 + \frac{2}{\gamma-1} \right) \quad (\text{A9})$$

$$\rho_* = r_* / (4\pi u_*) \quad (\text{A10})$$

$$P_* = 2\rho_* / \left[\gamma \left(M^2 + \frac{2}{\gamma-1} \right) \right] \quad (\text{A11})$$

for $r < R$ and

$$\rho_* = (4\pi r_*^2 u_*)^{-1} \quad (\text{A12})$$

but equations (A9) and (A11) as the same for $r > R$.

Furthermore, if we assume a power-law distributed q and Q for radius-dependent energy-injection and mass-loading efficiencies, i.e., $q \propto r^{-\xi}$ and $Q \propto r^{-\xi}$ with $\xi < 3$, the solutions for the Mach number M for $r < R$ becomes

$$\left[\frac{(\gamma-1) + 2/M^2}{\gamma+1} \right]^{(1+\gamma)/[2(1+5\gamma-\xi-\xi\gamma)]} \left[\frac{(3-\xi)\gamma + (1-\xi)/M^2}{(1-\xi) + (3-\xi)\gamma} \right]^{-(1+3\gamma-\xi-\xi\gamma)/[(1-\xi)(1+5\gamma-\xi-\xi\gamma)]} = \frac{r}{R}, \quad (\text{A13})$$

for $\xi \neq 1$, and

$$\left[\frac{(\gamma-1) + 2/M^2}{\gamma+1} \right]^{(1+\gamma)/8\gamma} \exp \left[\frac{1}{4\gamma} \left(1 - \frac{1}{M^2} \right) \right] = \frac{r}{R}, \quad (\text{A14})$$

for $\xi = 1$. And the dimensionless equation (A10) becomes

$$\rho_* = \frac{r_*^{1-\xi}}{4\pi u_*}, \quad (\text{A15})$$

while other solutions are the same as the case of the uniformly distributed q and Q . Using these models of $\xi \neq 0$, we have calculated the constraint on β for comparison with the results presented in this paper. For example, for the same R , SFR, f_d and $\alpha = 1$, but varying ξ from 0 to 3, we find that constraints on β for SFR $\gtrsim 1 M_\odot \text{ yr}^{-1}$ change by less than a factor of 50%. For a wide range of $\alpha \lesssim 2$, the basic conclusion in this paper that $\beta \lesssim 1$ for SFR $\gtrsim 10 M_\odot \text{ yr}^{-1}$ in the CC85 model is not changed.

REFERENCES

- Anders, E., & Grevesse, N. 1989, *GeCoA*, 53, 197
 Bower, R. G., Benson, A. J., & Crain, Robert A. 2012, *MNRAS*, 422, 2816
 Bradamante, F., Matteucci, F., & D'Ercole, A. 1998, *A&A*, 337, 338
 Chevalier, R. A., & Clegg, A. W. 1985, *Nature*, 317, 44
 Cantó, J., Raga, A. C., & Rodríguez, L. F. 2000, *ApJ*, 536, 896
 Cooper, J. L., Bicknell, G. V., Sutherland, R. S., & Bland-Hawthorn, J. 2008, *ApJ*, 674, 157
 Cooper, J. L., Bicknell, G. V., Sutherland, R. S., & Bland-Hawthorn, J. 2009, *ApJ*, 703, 330
 Dekel, A., & Silk, J. 1986, *ApJ*, 303, 39
 Dijkstra, M., Gilfanov, M., Loeb, A., & Sunyaev, R. 2012, *MNRAS*, 421, 213
 Elbaz, D., et al. 2007 *A&A*, 468, 33
 Everett, J. E., et al. 2008, *ApJ*, 674, 258
 Finlator, K., & Davé, R. 2008, *MNRAS*, 385, 2181
 Förster Schreiber, N. M., Genzel, R., Lutz, D., & Sternberg, A. 2003, *ApJ*, 599, 193
 Fujita, A., Martin, C. L., Mac Low, M.-M., et al. 2009, *ApJ*, 698, 693
 Gilfanov, M., Grimm, H.-J., & Sunyaev, R. 2004, *MNRAS*, 347, 57L
 Greco, J. P., Martini, P., & Thompson, T. A. 2012, *ApJ*, 757, 24
 Grimm H.-J., Gilfanov M., & Sunyaev R. 2003, *MNRAS*, 339, 793
 Heckman, T., Lehnert, M. D., Strickland D. K., & Lee, A. 2000, *ApJS*, 129, 493
 Hopkins, P. F., Quataert, E., & Murray, N. 2012, *MNRAS*, 421, 3522
 Kennicutt, R. C., Jr. 1998, *ARA&A*, 36, 189
 Lehmer, B. D., Alexander, D. M., Bauer, F. E., Brandt, W. N., Goulding, A. D., Jenkins, L. P., Ptak, A., & Roberts, T. P. 2010, *ApJ*, 724, 559
 Lehnert, M. D., & Heckman, T. M. 1996, *ApJ*, 472, 546
 Leitherer, C., et al. 1999, *ApJS*, 123, 3
 Lidders, K., Palme, H., & Gail, H.-P. 2009, *LanB*, 444
 Martin, C. L. 2005, *ApJ*, 621, 227
 Martin, C. L., Kobulnicky, H. A. & Heckman, T. M. 2002, *ApJ*, 574, 663
 McDowell, J. C. et al. 2003, *ApJ*, 591, 154
 Meurer, G. R., Heckman, T. M., Lehnert, M. D., Leitherer, C., & Lowenthal, J. 1997, *AJ*, 114, 54
 Melo, V. P., Pérez García, A. M., Acosta-Pulido, J. A., Muñoz-Tuñón, C., & Rodríguez Espinosa, J. M. 2002, *ApJ*, 574, 709
 Mineo S., Gilfanov M., & Sunyaev R., 2011, *Astron. Nachr.*, 332, 349
 Mineo, S., Gilfanov, M., & Sunyaev, R. 2012, *MNRAS*, 419, 2095
 Mineo, S., Gilfanov, M., & Sunyaev, R. 2012, *MNRAS*, 426, 1870
 Mineo, S., Gilfanov, M., & Sunyaev, R. 2014, *MNRAS*, 437, 1698
 Murray, N., Quataert, E., & Thompson, T. A. 2005, *ApJ*, 618, 569
 O'Connell, R. W., & Mangan, J. J. 1978, *ApJ*, 221, 62
 Oppenheimer, B. D., & Davé, R. 2006, *MNRAS*, 373, 1265
 Oppenheimer, B. D., & Davé, R. 2008, *MNRAS*, 387, 577
 Panuzzo, P., et al. 2010, *A&A*, 518, 37
 Ptak, A., Heckman, T., Levenson, N. A., Weaver, K., & Strickland, D. 2003, *ApJ*, 592, 782
 Persic, M., & Rephaeli, Y. 2007, *A&A*, 463, 481
 Puchwein, E., & Springel, V. 2013, *MNRAS*, 428, 2966
 Ranalli P., Comastri A., & Setti G. 2003, *A&A*, 399, 39
 Sanders, D. B., Mazzarella, J. M., Kim, D.-C., Surace, J. A., & Soifer, B. T. 2003, *AJ*, 126, 1607
 Schure, K. M., Kosenko, D., Kaastra, J. S., Keppens, R., & Vink, J. 2009, *A&A*, 508, 751
 Shlykovskiy, P., Gilfanov, M. 2005, *MNRAS*, 362, 879
 Strickland, D. K., Heckman, T. M., Weaver, K. A., & Dahlem, M. 2000, *AJ*, 120, 2965
 Strickland, D. K., Ponman, T. J., & Stevens, I. R. 1997, *A&A*, 320, 378
 Silich, S., Tenorio-Tagle, G., & Muñoz-Tuñón, C. 2003, *ApJ*, 590, 791
 Silich, S., Tenorio-Tagle, G., & Rodríguez-González, A. 2004, *ApJ*, 610, 226
 Socrates, A., Davis, S. W., & Ramirez-Ruiz, E. 2008, *ApJ*, 687, 202
 Springel, V., & Hernquist, L. 2003, *MNRAS*, 339, 289

- Stevens, I. R., & Hartwell, J. M. 2003, MNRAS, 339, 280
- Strickland, D. K., Heckman, T. M., Colbert, E. J. M., Hoopes, C. G., & Weaver, K. A. 2004, ApJ, 606, 829
- Strickland, D. K., & Heckman, T. M. 2007, ApJ, 658, 258
- Strickland, D. K., & Heckman, T. M. 2009, ApJ, 697, 2030
- Strickland, D. K., & Stevens, I. R. 2000, MNRAS, 314, 511
- Sutherland, R. S., & Dopita, M. A. 1993, ApJS, 88, 253
- Tenorio-Tagle, G., Wünsch, R., Silich, S., & Palouš, J. 2007, ApJ, 658, 1196
- Wang, J. et al., 2013, arXiv: 1303.2980
- Weaver, K. A., Heckman, T. M., Strickland, D. K., & Dahlem, M. 2002, ApJ, 576, 19L
- Wünsch, R., Tenorio-Tagle, G., Palouš, J., & Silich, S. 2008, ApJ, 683, 683
- Wünsch, R., Silich, S., Palouš, J.; Tenorio-Tagle, G., & Muñoz-Tuñón, C. 2011, ApJ, 740, 75